Chinese Journal of Aeronautics, (2018), 31(2): 255–261

Chinese Society of Aeronautics and Astronautics
& Beihang University

Chinese Journal of Aeronautics

cja@buaa.edu.cn
www.sciencedirect.com

Shock/shock interactions between bodies and wings

Gaoxiang XIANG [a,b], Chun WANG [b,*], Honghui TENG [b], Zonglin JIANG [b]

[a] School of Mechanics, Civil Engineering & Architecture, Northwestern Polytechnical University, Xi'an 710129, China
[b] Institute of Mechanics, Chinese Academy of Sciences, Beijing 100190, China

Received 4 August 2016; revised 6 January 2017; accepted 15 March 2017
Available online 5 December 2017

KEYWORDS

Body and wing;
Flow field;
Hypersonic flow;
Shock/shock interaction;
Wave configurations

Abstract This paper examines the Shock/Shock Interactions (SSI) between the body and wing of aircraft in supersonic flows. The body is simplified to a flat wedge and the wing is assumed to be a sharp wing. The theoretical spatial dimension reduction method, which transforms the 3D problem into a 2D one, is used to analyze the SSI between the body and wing. The temperature and pressure behind the Mach stem induced by the wing and body are obtained, and the wave configurations in the corner are determined. Numerical validations are conducted by solving the inviscid Euler equations in 3D with a Non-oscillatory and Non-free-parameters Dissipative (NND) finite difference scheme. Good agreements between the theoretical and numerical results are obtained. Additionally, the effects of the wedge angle and sweep angle on wave configurations and flow field are considered numerically and theoretically. The influences of wedge angle are significant, whereas the effects of sweep angle on wave configurations are negligible. This paper provides useful information for the design and thermal protection of aircraft in supersonic and hypersonic flows.

1. Introduction

In aerospace engineering, the prediction of aerodynamic heating is very important for the design of supersonic or hypersonic aircraft. There are two approaches to estimate aerodynamic heating in protective engineering. The first method is to use correlations between pressure and heating to predict the aerodynamic heating, which assumes that the aerodynamic heating is positively related to the pressure or density.[1] This approach is applied to the simple geometric shapes well; however, it could not predict the aerodynamic heating well for the complex geometric shape. The second method considers the location of Shock/Shock Interaction (SSI) or the interactive wave configuration as the key factors of aerodynamic heating [2], but the mechanism has not been well established. Thus, the problem of SSI is very important to the prediction of aerodynamic heating.

Regarding the SSI induced by the body and wing of aircraft, many researchers have conducted numerous experimental and numerical studies.[3–7] Zheltovodov and Schulein[3–5] conducted experimental and theoretical (computational) investigations on a model of one fin mounted on a flat plate at Mach number 3, and the technology of surface oil flow and flow visualization by Planar Laser Scattering (PLS) was used in his experiments. He also considered the effects of the deflec-

* Corresponding author.
E-mail address: wangchun@imech.ac.cn (C. WANG).

Peer review under responsibility of Editorial Committee of CJA.

Production and hosting by Elsevier

https://doi.org/10.1016/j.cja.2017.11.012

tion angle of the fin on surface pressure and wave configuration. Horstman and Hung[6] used the Reynolds-Averaged Navier–Stokes (RANS) simulation with a simple algebraic eddy-viscosity turbulence model to compute streamline trajectory. Schülein[7] performed experiments to study the surface pressure and skin-friction distributions at Mach number 5. Other researchers also study the SSI by using different models.[8–15] In the above research, the plate was flat and only the Shock wave-Boundary-Layer Interactions (SBLIs) were taken into consideration. In the design of hypersonic aircraft, the high heat flux may be caused by SSI and SBLIs. Therefore, the interactions between incident waves induced by the plate and the fin are very important for the prediction of heat flux in these regions.

Compared to the experimental and numerical researches, the theoretical research is seldom conducted. The earliest theories about 2D Regular Reflection (RR) and Mach Reflection (MR) were proposed by von Neumann,[16,17] who termed them as the two-shock theory and three-shock theory. Based on these theories, Kawamura and Saito[18] developed the (p, θ)-polar method, where p denotes the flow static pressure and θ is the flow deflection angles, to describe the shock reflection and SSI problems. Ben-Dor[19] used the (p, θ)-polar method to analyze various shock reflection and interaction wave configurations. However, the above theories are 2D, and in fact, there is no theory for the 3D cases. Recently, Yang and Xiang et al. developed a spatial dimension reduction approach to analyze the 3D SSI.[20–24] Through the use of the new theoretical method, the 3D steady SSI problem can be treated as a 2D unsteady one, and then, the flow structures could be solved by shock dynamic.

In this paper, the SSIs induced by bodies and wings were studied numerically and theoretically. The spatial dimension reduction method is used to analyze the flow parameter and the results are compared with the numerical results. In Section 2, the procedures and numerical methods are simply presented. Numerical results and theoretical analysis are given and discussed in detail in Section 3. Finally, the conclusions are drawn in Section 4.

2. Analytical approach and numerical methods

As depicted in Fig. 1, the numerical model is a simplified symmetrical model of a wing and body, where the body is replaced by a wedge and the wing is assumed to be a sharp wing. The wedge angle of the body is θ, and the body is L in length, d in width and h in height. The distance from the front point of the wing O to the leading edge of the body is l_1, A is the top point of the wing. λ_2 is the sweep angle of the wing, and is formed by the leading edge of the wing and the horizontal line. Half angle of the wedge is defined as θ_1, and the height of the wing is h_1.

For the free inviscid inflow Ma_0, the incident wave CBF is induced by the body, the incident wave APR is induced by the wing, and they interact with each other in the corner as shown in Fig. 2. Two reflected waves, OPR and PRG, occur due to the intersection of the two incident waves. The computational zone is selected as half of the model, which is divided by the symmetry plane. The intersecting line of the two incident waves, PR, is defined as the characteristic direction, and the plane NMD perpendicular to it is defined as the characteristic plane. Q is the intersecting point of line PR and the plane NMD. In the interactive zone, the wave configuration is self-similar in the direction of the characteristic line, and thus, the 3D steady SSI could be regarded as a 2D SSI in the characteristic plane moving in the direction of the characteristic line PR.

The decomposed Mach number projected on PR is Ma_n. The decomposed Mach numbers Ma_{s1} and Ma_{s2} on the characteristic plane are given by

$$Ma_{s1} = Ma_0 \sin\beta_1, \quad Ma_{s2} = Ma_0 \sin\beta_{2n} \cos\lambda_2 \tag{1}$$

where β_1 is the shock angle in the direction of the incoming flow, and β_{2n} is the shock angle perpendicular to the leading edge of the wing.

When the above geometrical relationships between 3D steady problem and 2D unsteady problem are determined, the problem of 3D could be regarded as the interaction of two incident waves Ma_{s1} and Ma_{s2} moving on the characteristic plane, which can be treated as the characteristic plane moving in the direction of the characteristic line PR.

The determination of the wave configurations could be achieved by shock polar analysis of the 2D unsteady problem.[18,19]

$$\tan\theta = \frac{\xi - 1}{\gamma Ma^2 - (\xi - 1)} \sqrt{\frac{\frac{2\gamma}{\gamma+1}(Ma^2 - 1) - (\xi - 1)}{\xi + \frac{\gamma - 1}{\gamma + 1}}} \tag{2}$$

where Ma is the decomposed Mach number in the direction of the reflection point, γ is 1.4 for an ideal gas, and ξ is the ratio of the pressure behind the waves.

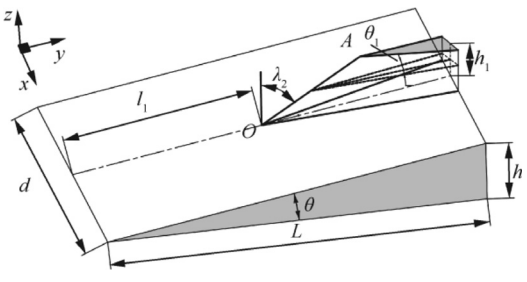

Fig. 1 Schematic illustration of a simplified model for wing and body.

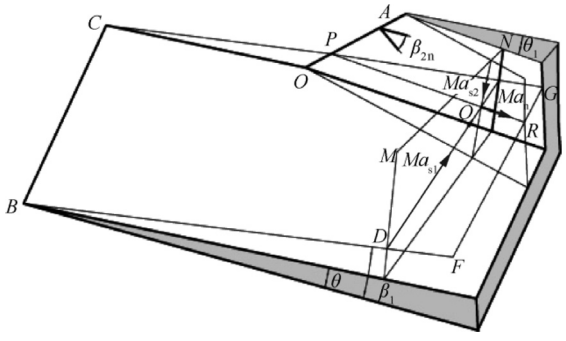

Fig. 2 Schematic of "spatial-dimension reduction" approach.

If the wave configuration is Mach interaction, a Mach stem is formed between Ma_{s1} and Ma_{s2}. The Mach number behind the Mach stem Ma_m and the location of the Mach stem can be given by the shock dynamics.[25,26]

$$\tan\theta_v = \frac{Ma_m}{Ma_{s2}} \cdot \frac{\left[1-\left(\frac{Ma_{s2}}{Ma_m}\right)^2\right]^{\frac{1}{2}}\left\{1-\left[\frac{f(Ma_m)}{f(Ma_{s2})}\right]^{\frac{1}{2}}\right\}}{1+\frac{f(Ma_m)Ma_m}{f(Ma_{s2})Ma_{s2}}} \tag{3}$$

$$\tan(\pi-\eta-\theta_v) = \frac{Ma_m}{Ma_{s1}} \cdot \frac{\left[1-\left(\frac{Ma_{s1}}{Ma_m}\right)^2\right]^{\frac{1}{2}}\left\{1-\left[\frac{f(Ma_m)}{f(Ma_{s1})}\right]^{\frac{1}{2}}\right\}}{1+\frac{f(Ma_m)Ma_m}{f(Ma_{s1})Ma_{s1}}} \tag{4}$$

Here, $f(Ma)$ is a function in terms of the Mach number Ma. θ_v is the angle between the virtual wall and the horizontal line. η is the angle between two incident waves. Then, all the parameters in the 2D flow field could be obtained. For the 3D flow field, the state parameters, such as the temperature, pressure, density and the total pressure recovery coefficient, are identical to those of the 2D unsteady solutions. The vector parameters, such as the velocities and Mach number, should be composed with the decomposed vectors in the direction of the characteristic line.

For the numerical computations, the 3D inviscid Euler equations of a perfect compressible gas were solved. The code was developed at the Shock Wave and Detonation Physics Laboratory and run on a DELL 8-core computer. It used a Non-oscillatory and Non-free-parameters Dissipative finite difference (NND) scheme,[27] which was based on an orthogonalized uniform structured mesh, with a mesh number of $120 \times 200 \times 200$ in the x, y and z directions. The Message Passing Interface (MPI) parallel program was used in the code. Mesh independent tests were performed to ensure that all the results produced were independent of the type of mesh chosen for the numerical simulations.

3. Presentation of results

In this section, theoretical and numerical researches are conducted to explore the impacts of geometric parameters on the flow field and wave configuration. Due to the symmetry of the model, only half of the general numerical simulations are carried out. The coming flow Mach number is selected as 7.03, and the geometric parameters of wing and body for the numerical computations are listed in Table 1. In order to study the effects of the thickness of the wing, Cases 1 to 3 are conducted at wedge angle θ_1 of 2°, 5° and 10°, where the other parameters are fixed at $\lambda_2 = 30°$, $L = 1200$ mm, $d = 500$ mm, $h_1 = 350$ mm, $l_1 = 500.9$ mm, $\theta = 3.5°$. In Cases 1, 4 and 5, the sweep angle varies from 30° to 60°, and other parameters are fixed.

For the Cases 1 to 5, the incident wave induced by the body intersects with the incident wave induced by the wing, and several of the wave configurations are formed. When the height of the wing h_1 is sufficiently small (see Case 6 and Fig. 3), the incident wave induced by the body does not intersect the incident wave induced by the wing, and the high heat flux induced by the SSI on the side of the wing does not occur. In this situation, the expansion waves induced by the wall of the wing form in order to match the two incident waves and make the incident waves induced by the wing curved.

3.1. Effects of wedge angle of wing

The wedge angle of the wing corresponds to the thickness of the wing (Fig. 1), which is a key parameter for designing the aircraft. For Cases 1 to 3, shock polar analysis on the cross-section indicates that the two reflected polar do not intersect each other and it means that a Mach interaction will occur in the side of the wing (Fig. 4(a)). As depicted in Fig. 4(a), when the wedge angle of the wing increases, two incident polar I_i, and I_i', and the reflected polar R_i near the body grow bigger and higher, while the reflected polar R_i near the wing becomes smaller and changes into a point at $\theta_1 = 10°$, which implies that the flow behind the incident wave on the characteristic plane is subsonic and the (p, θ) polar does not exist. When the reflected polar is totally on the incident polar or recessed into one point, it means that the reflection is a weak reflection and the reflected wave degenerates into an expansion wave on this side (Fig. 4(d)).

The salient feature of hypersonic interactions is the occurrence of high heat transfer rates in the interaction region, which consists of the domain of SBLIs and SSI. In this paper, the viscosity is negligible, while the location of the SBLIs induced by the reflected wave and the boundary layer can be predicted using the inviscid results (Fig. 4(b)–(d)). The intersecting point of the wall boundary and the reflected wave gets farther in the positive direction of the x and z axes as θ_1 increases (Figs. 4(b)–(d), 5, 8 and 4, 7). It should be noted that the reflected wave near the wing changed into an expansion wave at $\theta_1 = 10°$, and the intersecting point almost reaches the top of the wing, where the thermal protection should be considered. Compared to the wing, the location of the reflected wave on the wall boundary on the side of the body changed

Table 1 Geometric parameters of wing and body in numerical computations.

Case	θ_1 (°)	λ_2 (°)	L (mm)	d (mm)	h_1 (mm)	l_1 (mm)	θ (°)
1	2	30	1200	500	350	500.9	3.5
2	5	30	1200	500	350	500.9	3.5
3	10	30	1200	500	350	500.9	3.5
4	2	45	1200	500	350	500.9	3.5
5	2	60	1200	500	350	500.9	3.5
6	5	45	1200	500	110	500.9	3.5

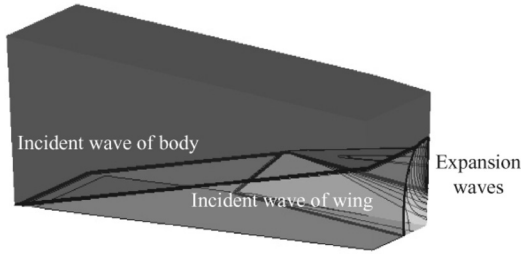

Fig. 3 Numerical result for case 6.

slowly in the positive direction of the axis. Another region of high heat flux is caused by the SSI behind the Mach stem 3. This zone grows larger with the increase of θ_1 due to the increasing length of the Mach stem. The high heat flux region forms by the slip line 6 and the Mach stem gets larger with the increase of θ_1.The temperature and pressure behind the Mach stem can be solved by the spatial dimension reduction approach.

As shown in Fig. 5(a) and (b), the abscissa axis is the varying wedge angle of the wing θ_1, and the vertical axis is the parameter ratio behind the Mach stem (T_b, P_b) and in front of the Mach stem (T_f, P_f). As illustrated in Fig. 5, the theoretical solutions in the vicinity of the Mach stem are in good agreement with the numerical results. The temperature ratio and pressure ratio gradually increase with the increasing thickness of the wing. The temperature behind the Mach stem T_b is about twice that of the inflow, and the pressure is about five times that of the inflow. Accordingly, the SSI in the distance should not be ignored in the design of aircraft.

3.2. *Effects of sweep angle of wing*

The impacts of the sweep angle λ_2 are investigated here using examples of Cases 1, 4 and 5. The evolution of the

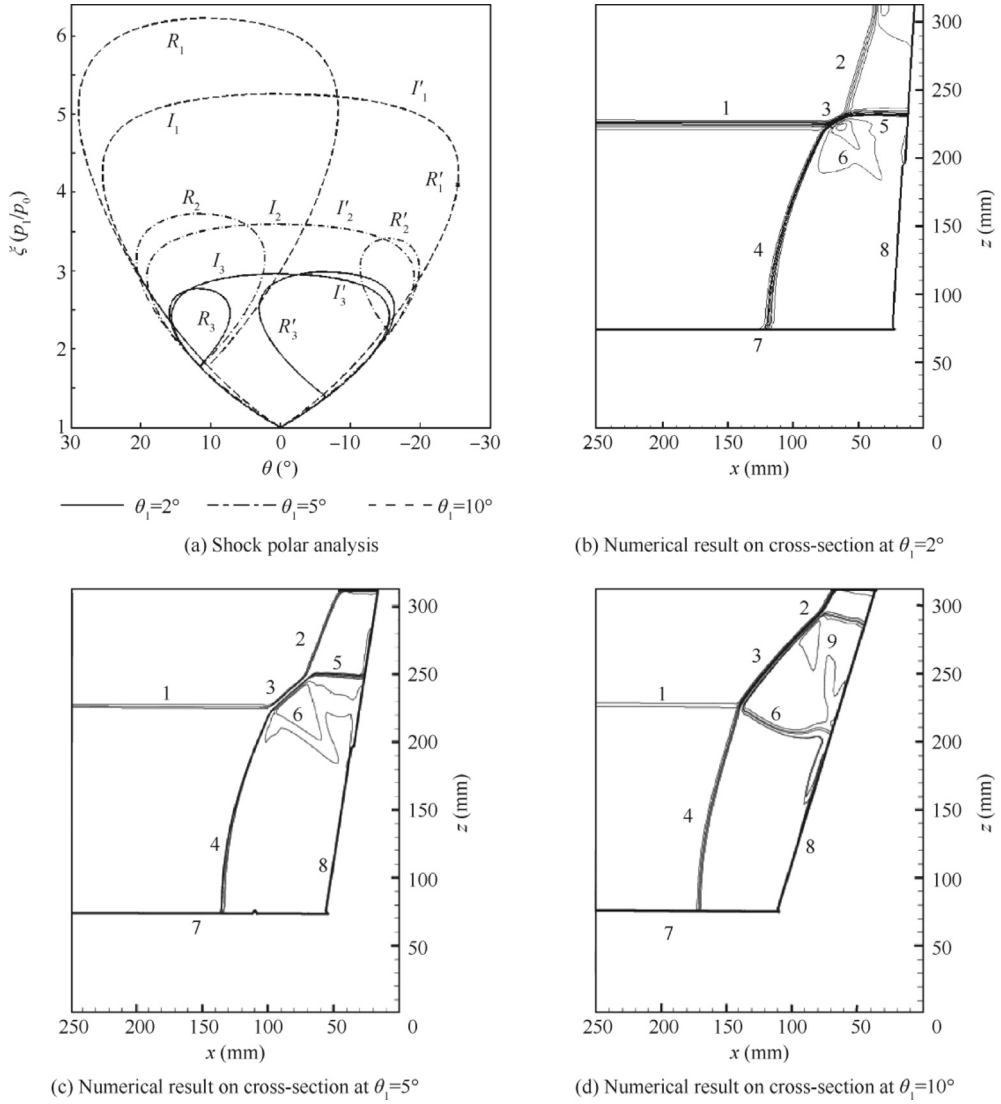

Fig. 4 Analytical and numerical results for varying wedge angle of wing at y = 1200 mm (Note: 1— incident wave of body; 2—incident wave of wing; 3—Mach stem; 4—reflected wave near body; 5—reflected wave near wing; 6—slip line; 7—wall boundary of body; 8—wall boundary of wing; 9—expansion fan near wing).

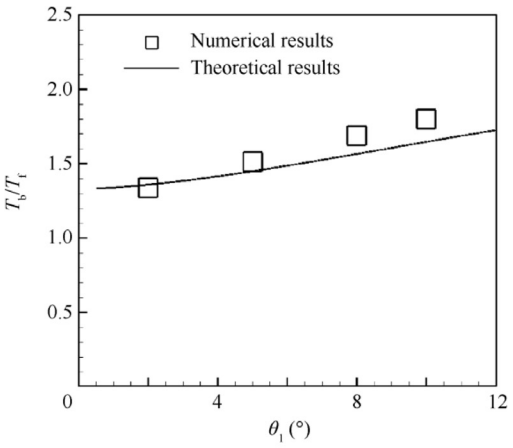

(a) Temperature behind Mach stem 3

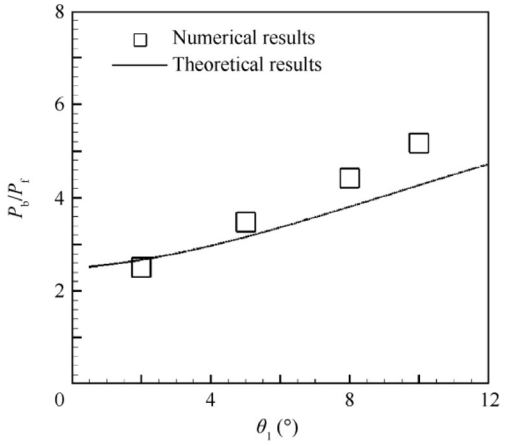

(b) Pressure ratio behind Mach stem 3

Fig. 5 Analytical and numerical results after varying wedge angle of wing.

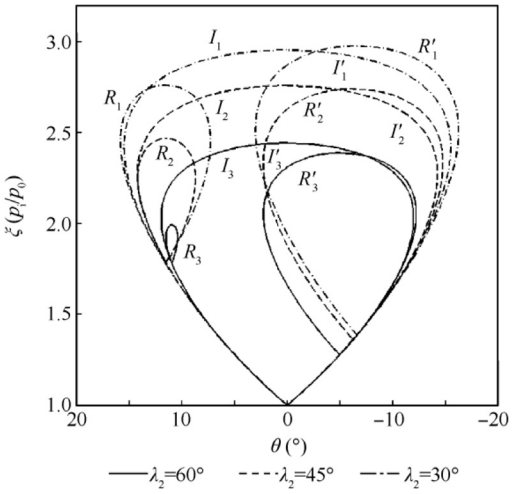

Fig. 6 Shock polar analysis after varying sweep angle of wing at y = 1200 mm.

shock-polar analysis on the cross-sections at λ_2 = 30°, 45°and 60° is shown in Fig. 6. As λ_2 increases, the incident polar and

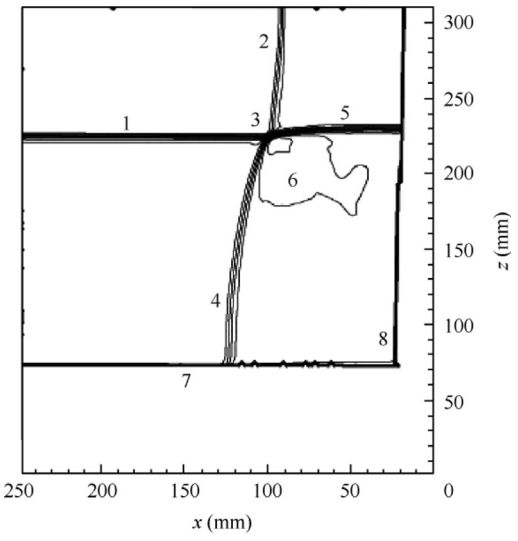

(a) Numerical result on cross-section at λ_2=10°

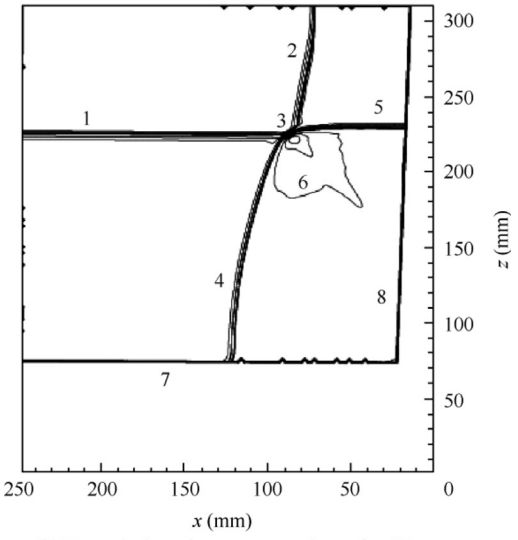

(b) Numerical result on cross-section at λ_2=60°

Fig. 7 Numerical results after varying sweep angle of wing at y = 1200 mm.

the reflected polar get smaller and lower, where the two reflected polar do not interact with each other, indicating that the wave configurations are Mach interactions. The corresponding cross-sectional flow structures are shown in Figs. 4 (b) and 7(a) and (b).

Compared with θ_1, the effects of λ_2 on the wave configurations are negligible. The increase of the sweep angle does not cause any obvious change on the location of the reflected waves and the Mach stem. This means that the region of high heat flux induced by the SSI and SBLIs changes very slowly with the varying sweep angle λ_2. However, for the high heat transfer rate behind the Mach stem, the sweep angle exhibits the opposite tendency, where the increase of λ_2 leads to a reduction of the pressure and temperature behind the Mach stem (see Fig. 8(a) and (b)). The results shown in Figs. 5 and 8 reveal that the impacts of the sweep angle on pressure and temperature are smaller than those of the wedge angle.

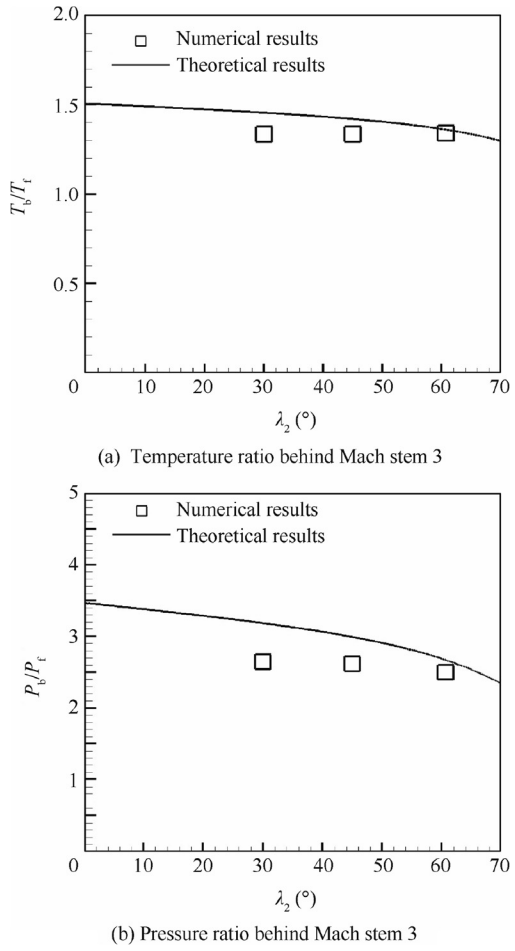

Fig. 8 Analytical and numerical results after varying sweep angle of wing.

4. Conclusions

(1) In this study, the method of spatial dimension reduction is applied to study the SSI induced by the bodies and the wings. The wave configuration can be determined by shock polar analysis on the cross-section, and the flow field parameters in the vicinity of the Mach stem can be predicted by this method, which are in good agreement with the numerical results. The location of the high heat flux caused by the interaction with the reflected wave and the boundary layer can be predicted by the inviscid results.

(2) If the incident wave of the body interacts with the incident wave of the wing, several wave configurations occur in the interactive region. However, if the height of the wing is sufficiently small or the wedge angle of the body is larger, the two incident waves do not interact with each other and an expansion fan is formed at the top of the wall of the wing.

(3) As the wedge angle of the wing increases, the pressure and high heat flux behind the Mach stem induced by the SSI clearly rise up obviously, while the area that is formed by the Mach stem and slip lines gets bigger due to the increasing length of the Mach stem. The flow field parameters behind the Mach stem exhibit the opposite trend with the increase of the sweep angle of the wing, and the impacts can be considered negligible compared with the wedge angle.

(4) For the sufficiently large wedge angle of the wing, the wave configuration is a weak reflection. The reflected wave near the wall of the wing changes into an expansion fan according to the theoretical and numerical analyses, and the impacts can be considered negligible compared with the wedge angle. The intersecting point of the wall boundary and the reflected waves get farther in the positive direction of x and z axes as the wedge angle of the wing increases. However, this intersecting point changes little with the increase of the sweep angle.

Acknowledgements

The authors would like to thank Prof. LUO CT and HU ZM for their valuable assistance. This paper is supported by the Fundamental Research Funds for the Central Universities of China (No. 31020170QD087).

References

1. Neumann RD, Burke GL. The influence of shock wave-boundary layer effects on the design of hypersonic aircraft. Wright-Patterson AFB: Air Force Flight Dynamics Lab; 1969. Report No.: AFFDL-TR-68-152.
2. Edney B. Anomalous heat transfer and pressure distributions on blunt bodies at hypersonic speeds in the presence of an impinging shock. Stockholm: The Aeronautical Research Institute of Sweden; 1968. Report No.: FFA-115.
3. Zheltovodov AA. Some advances in research of shock wave turbulent boundary-layer interactions. Reston: AIAA; 2006. Report No.: AIAA-2006-0496.
4. Zheltovodov AA. Shock waves/turbulent boundary-layer interactions—Fundamental studies and applications. Reston: AIAA; 1996. Report No.: AIAA-1996-1977.
5. Zheltovodov AA, Schulein E. Three-dimensional swept shock waves/turbulent boundary layer interaction in angle configurations. Novosibirsk: USSR Academy of Sciences; 1986 [Russian].
6. Horstman CC, Hung CM. Computation of three-dimensional turbulent separated flows at supersonic speeds. *AIAA J* 1979;**17**(11):1155–6.
7. Schülein E. Skin friction and heat flux measurements in shock/boundary layer interaction flows. *AIAA J* 2006;**44**(8):1732–41.
8. Wang C, Xiang GX, Jiang ZL. Theoretical approach to one-dimensional detonation instability. *Appl Math Mech* 2016;**37**(9):1231–8.
9. Hu ZM, Wang C, Zhang Y, Myong RS. Computational confirmation of an abnormal Mach reflection wave configuration. *Phys Fluids* 2009;**21**(1):011702.
10. Zhai ZG, Wang MH, Si T, Luo XS. On the interaction of a planar shock with a light polygonal interface. *J Fluid Mech* 2014;**757**:800–16.
11. Zhai ZG, Si T, Luo XS, Yang JM. On the evolution of spherical gas interfaces accelerated by a planar shock wave. *Phys Fluids* 2011;**23**:84–104.
12. Zhai ZG, Liu CL, Qin FH, Yang JM, Luo XS. Generation of cylindrical converging shock waves based on shock dynamics theory. *Phys Fluids* 2010;**22**:041701.
13. Xue XP, Nishiyama Y, Nakamura Y, Mori K, Wang YP, Wen CY. High-speed unsteady flows past two-body configurations. *Chinese Journal of Aeronautics* 2018;**31**(1):54–64.

14. Wang HY, Li J, Jin D, Dai H, Gan T, Wu Y. Effect of a transverse plasma jet on a shock wave induced by a ramp. *Chin J Aeronaut* 2017;**30**(6):1854–65.
15. Chen ZJ, Lin J, Bai CY, Wu ZN. A self-similar solution of a curved shock wave and its time-dependent force variation for a starting flat plate airfoil in supersonic flow. *Chin J Aeronaut* 2018;**31**(2):205–13.
16. von Neumann J. Refraction, interaction and reflection of shock waves. Washington, D.C.: U.S. Navy, Bureau of Ordnance; 1943. Report No.: 203-45.
17. von Neumann J. *Oblique reflection of shock waves*. Oxford: Pergamon Press; 1996.
18. Kawamura R, Saito H. Reflection of shock waves—1 Pseudo-stationary case. *J Phys Soc Jpn* 1956;**11**(5):584–92.
19. Ben-Dor G. *Shock wave reflection phenomena*. 2nd ed. Berlin: Springer-Verlag; 2007. p. 134–93.
20. Yang Y, Wang C, Jiang ZL. Analytical and numerical investigations of the reflection of asymmetric nonstationary shock waves. *Shock Waves* 2012;**22**(54):435–49.
21. Xiang GX, Wang C, Teng HH, Jiang ZL. Study on Mach stems induced by interaction of planar shock waves on two intersecting wedges. *Acta Mech Sinica* 2016;**32**(3):362–8.
22. Xiang GX, Wang C, Teng HH, Jiang ZL. Investigations of three-dimensional shock/shock interactions over symmetrical intersecting wedges. *AIAA J* 2016;**54**(5):1–10.
23. Xiang GX, Wang C, Hu ZM, Jiang ZL. Theoretical solutions to three-dimensional asymmetrical shock/shock interaction. *Sci China Technol Sci* 2016;**59**(8):1208–16.
24. Xiang G, Wang C, Teng H. Three-dimensional shock wave configurations induced by two asymmetrical intersecting wedges in supersonic flow. *Shock Waves* 2017;**1**:1–9.
25. Yang Y. Analytical and numerical investigations of the reflection of asymmetric nonstationary shock waves. *Shock Waves* 2012;**22**(5):435–49.
26. Xie P. A study of the interaction between two triple points. *Shock Waves* 2005;**14**(1):29–36.
27. Zhang HX. A dissipative difference scheme of non-oscillatory, no-free parameters. *Acta Aerodynamica Sinica* 1988;**6**(2):143–65 [in Chinese].